Optimizing the electronics for antiproton trapping at the BASE collaboration

Author: Rafael Agathangelou*,**
Supervisor: Prof. Dr. Stefan Ulmer**, Dr. Barbara Latacz**
June 16th - August 8th, 2025
*Department of Physics, University of Cyprus
**Baryon Antibaryon Symmetry Experiment, CERN

Abstract

This report summarizes the design and development of the electronics required for antiproton catching in the Reservoir Trap (RT) of the BASE collaboration at CERN. The project began with an in-depth review of the BASE trap stack and the role of the RT in enabling long-term storage of antiprotons for high-precision measurements during CERN accelerator shutdowns. Based on insights regarding the available power supplies and high-voltage switches, a tailored electronic circuit was designed, simulated, and developed to promptly deliver the fast, high-voltage pulses needed for precise antiproton trapping. The solution aimed to meet stringent requirements on noise suppression, timing accuracy, and integration within the existing infrastructure. The resulting electronics provide reliable, low-noise operation with tens of nanoseconds switching precision, crucial for the successful capture and long-term storage of antiprotons in BASE's RT system.

Key-words: Penning trap, Antimatter, Antiprotons, High-voltage switching, Fast-pulse electronics, CPT symmetry, Particle trapping

1 Introduction

Why our Universe is made almost entirely of matter, with hardly any antimatter left over, remains one of the biggest open questions in physics. According to the Standard Model and cosmological observations, matter and antimatter should have been created in equal amounts in the Big Bang. Tiny differences in their properties, if they exist, could explain why matter prevailed. Testing this requires comparing fundamental quantities of particles and their antiparticles to the highest possible precision.

The Baryon Antibaryon Symmetry Experiment (BASE) collaboration at CERN tackles this challenge by measuring the charge-to-mass ratio and the magnetic moment of protons and antiprotons in a Penning trap setup. A crucial element of this setup is the "reservoir trap," which catches low-energy antiprotons ($\sim 100\,\mathrm{keV}$) delivered by the ELENA decelerator and holds them stably for months. This lets the experiment run measurements on antiprotons during periods when antiproton beams are not available, as well as periods when other experiments are not running, greatly improving data collection efficiency due to the reduced background noise.

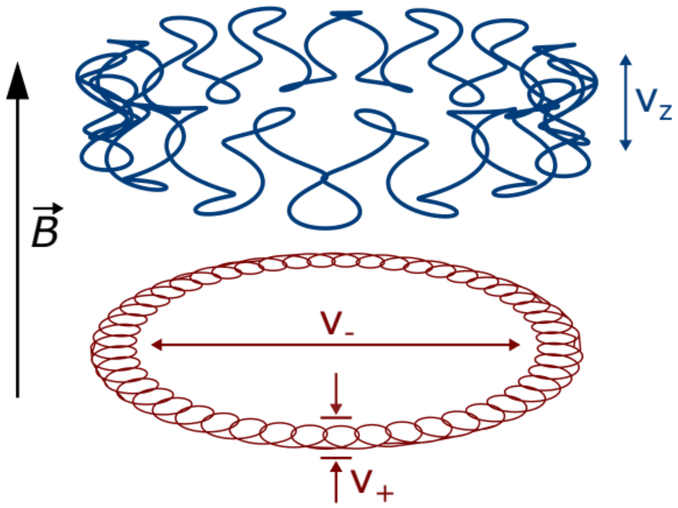

Fig. 1 Illustration of the trajectory of particles trapped in a cylindrical Penning trap. The particles undergo axial oscillation at frequency ν_z, radial motion composed of cyclotron (ν_+) and magnetron (ν_-) oscillations. The actual values of these frequencies follow the hierarchy $\nu_+ \gg \nu_z \gg \nu_-$. Adapted from Borchert M.J.[1]

In the Penning trap used at the BASE collaboration, partly shown in Fig. 2, a single charged particle is confined by a combination of a strong uniform magnetic field B ($\sim 2\,\mathrm{T}$) and an electrostatic quadrupole potential. Its motion separates into three eigenfrequencies, the modified cyclotron frequency ν_+, the magnetron frequency ν_-, and the axial frequency ν_z, causing the trapped particle to follow the trajectory shown in Fig.

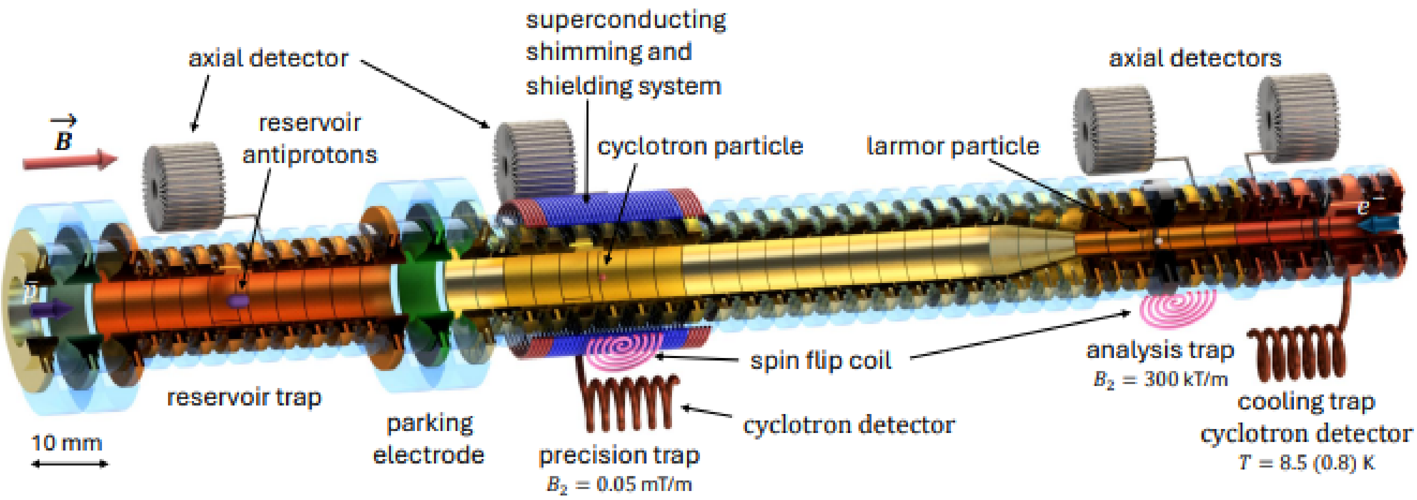

Fig. 2 The Penning-trap stack used by the BASE collaboration, including the reservoir trap (RT), precision trap (PT), analysis trap (AT) and cooling trap (CT). Antiprotons are stored in the RT and shuttled to the PT and AT for high-precision measurements. Adapted from the BASE 2024 annual report.[7]

1 in blue. These satisfy the "invariance theorem":

$$\nu_c^2 = \nu_+^2 + \nu_-^2 + \nu_z^2 \tag{1}$$

where ν_c is the free-space cyclotron frequency, given by:

$$\nu_c = \frac{qB}{2\pi m} \tag{2}$$

By measuring ν_+, ν_-, and ν_z, one can determine the charge-to-mass ratio $\frac{q}{m}$.

To measure the magnetic moment μ, spin-flip transitions are driven at the Larmor frequency:

$$\nu_L = \frac{gqB}{4\pi m} \tag{3}$$

This leads to the important ratio:

$$\frac{g}{2} = \frac{\nu_L}{\nu_c} \tag{4}$$

By comparing ν_L and ν_c, one obtains a direct, field-independent measurement of the g-factor. Comparing the g-factor and charge-to-mass ratio between protons and antiprotons allows for precision tests of CPT symmetry. A more detailed derivation and experimental procedure can be found in Borchert M.J.[1]

Reliably catching antiprotons for measurements demands extremely fast, high-voltage pulses on the trap electrodes, switching in just a few nanoseconds and without introducing excess electrical noise that could heat or eject the particles.

Over the course of the 2025 CERN Summer Student Program, I first reviewed the reservoir-trap electrode stack and the timing requirements for the catching sequence. I then designed, simulated, and laid out an improved high-voltage switching circuit, and finally built a prototype and measured its pulse-edge rise and fall times, as well as timing jitter and directly comparing these results to the simulations and required characteristics.

2 System overview and requirements

The key function of the reservoir trap (RT) is to enable the reliable capture and storage of antiprotons delivered by the ELENA decelerator. To achieve this, the electrodes adjacent to the RT are used to form fast-switchable potential barriers,[6] as illustrated in Fig. 3. In this configuration, two high-voltage electrodes—HVP (High Voltage Pulse) and HVS (High Voltage Static)—are positioned at either end of the trap, as shown in Fig. 2 on the left.

Initially, the HVS electrode is biased to a high negative voltage, forming a reflecting barrier, while the HVP electrode is held at ground to allow the incoming antiprotons to enter the trap. Once the antiproton bunch has entered the trap region, the HVP electrode is rapidly pulsed to a high negative voltage within a few nanoseconds, creating a second barrier and thereby closing the trap. This forms a potential well in which the antiprotons are confined longitudinally. After successful trapping, the caught antiprotons are then sympathetically cooled by electrons that were preloaded in the RT from the DS electrode.

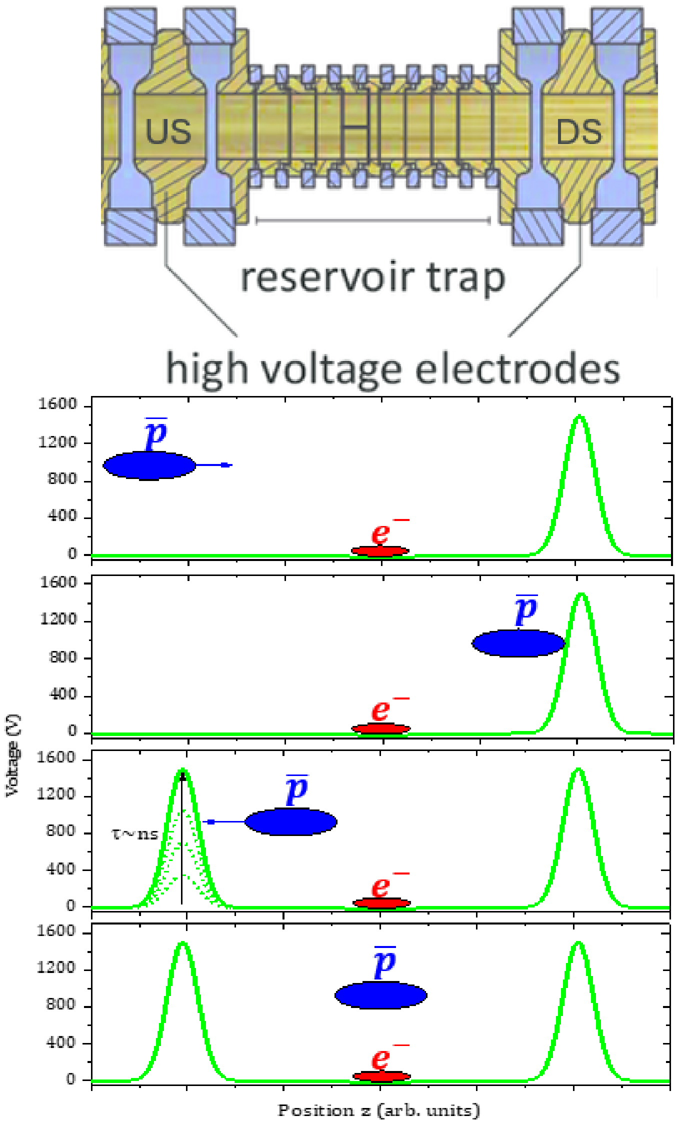

Fig. 3 Illustration of the dynamic potential configuration of the reservoir trap and adjacent electrodes during the antiproton catching process. Antiprotons are allowed in by lowering the HVP potential barrier and then trapped by quickly raising it after a delay trigger. The delay trigger is estimated based on the time-of-flight of the antiprotons, from their ejection from ELENA, to their reflection from the downstream (DS) potential barrier, to their second pass from the upstream (US) electrode.

Temporal requirements

Precise timing is critical to the antiproton catching process. As shown in Fig. 3, the upstream (US) barrier—controlled by the HVP electrode—must be raised at exactly the right moment to trap the antiprotons after they reflect from the downstream (DS) barrier. This moment is estimated based on the time-of-flight of the antiproton bunch, from its ejection by ELENA,to its first pass through the US electrode, through its reflection at the DS electrode and finally to its second pass through the HVP electrode. The total distance from the US to the DS electrode and back, in terms of antiproton velocity, is $\sim 90.6\,ns$, while the aniproton bunch has a length of $\sim 75\,ns$ before passing the degrader and a few μs after, meaning we raise the US-HV barrier while the bunch is flying in and out of the RT. Evidently, based on the time-of-flight within the RT and the bunch width, the rise time of the US-HV potential must be in the nanosecond regime to ensure that the trap closes while the entire bunch is still within the resrvoir trap, in order to maximize the number of caught antiprotons.

However, the actual trigger delay must also account for latency introduced by the electronics, particularly the response time of the HV switch responsible for raising the barrier.[3] Figure 4 provides the detailed time-of-flight breakdown. The antiproton bunch takes approximately 10.5 μs to reach the ELENA gate valve after ejection. Its total time-of-flight to the second pass through the HVP electrode is about 11.1 μs. Considering the switch's response time of approximately 250 ns, the actual trigger delay is corrected to ~10.8 μs after ejection.

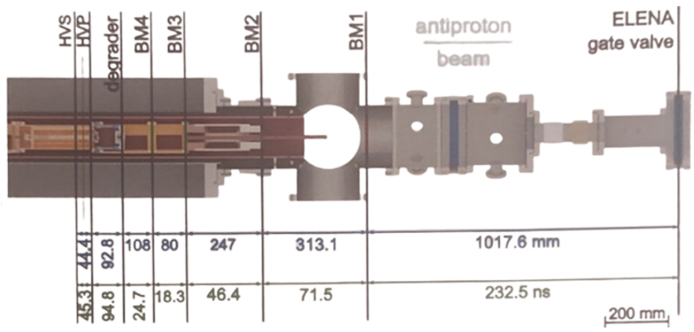

Fig. 4 Distance (blue) of the ELENA gate valve, beam monitors, and HV-electrodes of the RT in mm and the corresponding antiproton flight time (green) in ns for a 100 keV beam upstream of the degrader and 5 keV antiprotons downstream of the degrader.

It is also important to note that the RT HV barriers are typically biased to around 2 kV. Initially, the antiproton bunch has an energy of approximately 100 keV, which would allow it to bypass the barriers unimpeded. To address this, a degrader is positioned downstream of the gate valve to reduce the beam energy to roughly 5 keV, enabling effective trapping.[6] Since only a few antiprotons are needed for BASE measurements, capturing the lower-energy portion of the $\sim\mu$s long bunch, typicallt containing $\sim 3 \times 10^7$ antiprotons, is entirely sufficient.

Filtering and stability requirements

After the antiprotons have been successfully trapped in the RT, the stability of the electrostatic potential becomes crucial for long-term storage and high-precision measurements. During the catching process, a HV pulse, typically around 2 kV, is applied to the US electrode to create a fast potential barrier within nanosecond-scale timing. This voltage is delivered by a HV power supply such as the CAEN NDT1470, which can reach up to 8 kV, but has a relatively high output noise of up to 30 mV_{pp}.[4]

While such noise is tolerable during the brief catching phase, continued use of this noisy supply would compromise the stability of the trapping potential. Elevated noise levels can lead to unwanted heating of the antiprotons, increased axial motion, and potential particle loss. Moreover, the noise can interfere with the ultra-sensitive axial detection systems based on superconducting LC resonators,[3] degrading the signal-to-noise ratio of the measurements.

To mitigate this, the HV electrodes (HVP and HVS) are switched to a low-noise power supply immediately after trapping. Typically, a device such as the Stahl Electronics BSHV-400 is used, which can supply up to 400V with a maximum noise level of just 0.75 mV_{pp}.[5] Although the voltage is lower, it is sufficient to maintain the confinement of the now-cooled antiprotons (Fig. 3). The significant reduction in noise ensures electrostatic potential stability, which is essential for preserving the trapped particle cloud over long durations.

In addition to switching to low-noise high-voltage power supplies after antiproton catching, active filtering is necessary to ensure the long-term stability of the electrostatic potentials applied to the trap electrodes.[1,3] Power supplies used during the catching phase often introduce significant voltage ripple and high-frequency noise, which can result in electric field fluctuations. These fluctuations may lead to unwanted heating of the antiprotons, increased axial motion, and potential particle loss from the reservoir trap. One example of the danger of electric field fluctuations leading to motional heating and particle loss is described in Ulmer et al. 2018.[6] Moreover, they can interfere with the resonator-based detection systems, degrading the signal-to-noise ratio and the accuracy of precision measurements.

To suppress high-frequency noise and transient spikes from the power supplies, a dedicated filter must be introduced between the output of the HV supply and the trap electrodes. This filter must fulfill the following requirements:[1,2,6]

- **Noise suppression:** Attenuate high-frequency components and voltage ripple to minimize electromagnetic interference.
- **Spike protection:** Block or suppress fast voltage transients that could disturb the trap.
- **Current isolation:** Prevent backflow into sensitive electronics during HV switching.
- **Dual compatibility:** Support both fast HV pulses (for catching) and stable DC operation (for storage).

Ensuring these conditions is essential for preserving trap integrity and enabling precision measurements over extended timescales.

Board layout constraints for high-voltage

Designing PCBs for high-voltage operation (up to 2 kV in this system) requires layout strategies that prevent sparking, surface leakage, and dielectric breakdown. Adequate clearance must be maintained between conductive elements to account for the high potential differences involved.

Trace widths are increased to lower electric field intensity and support potential current surges. Sharp corners on traces and pads are avoided, as they can concentrate electric fields and trigger discharge. Lastly, a solder mask should be used to suppress surface leakage currents, while leaving critical soldering areas uncovered.

These design choices are consistent with layout strategies used in previous high-voltage boards developed for antiproton catching in the BASE collaboration,[3] and they help ensure electrical robustness under both fast HV switching and steady bias conditions.

3 Design and Implementation

To fulfill the timing, filtering, and stability requirements outlined above, a tailored circuit was designed to drive the high-voltage electrodes (HVP and HVS) of the reservoir trap. The goal was to deliver fast, high-voltage pulses with nanosecond-scale rise times, while maintaining low noise during static confinement. The full schematic of the design is shown in Fig. 5. The circuit is centered around a high-voltage relay-based switching stage, which enables fast toggling between

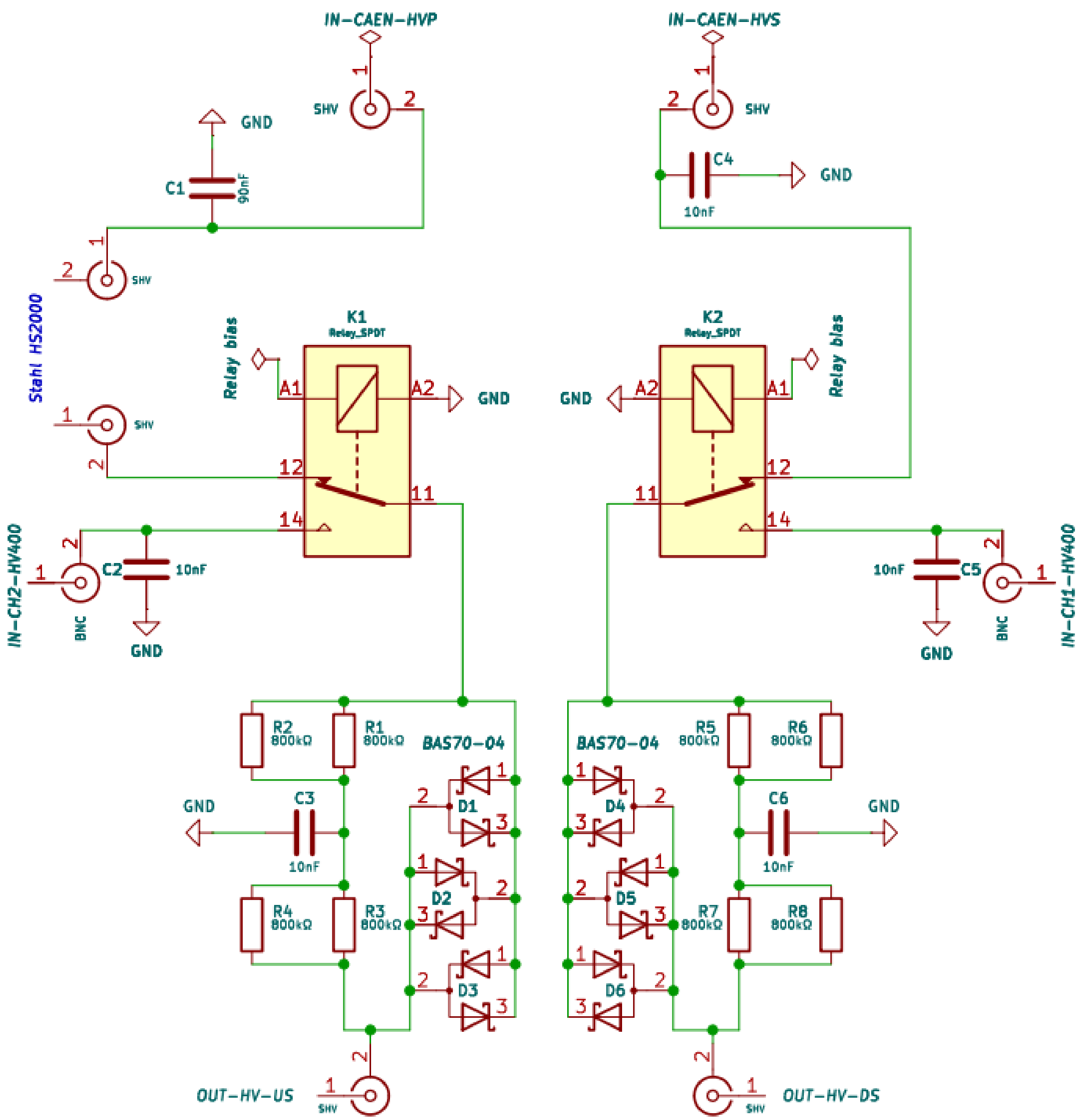

Fig. 5 Tailored schematic of the electronics developed for delivering fast, high-voltage pulses to the US and DS HV electrodes of the BASE reservoir trap. The circuit was designed in KiCAD 9.0 to meet the timing and stability requirements necessary for efficient antiproton trapping.

two power sources: a noisy but fast HV pulse supply (e.g. CAEN NDT1470), and a low-noise DC supply (e.g. Stahl BSHV-400) used for long-term storage. The switching configuration ensures that immediately after trapping, the trap electrodes are connected to the quieter source without introducing switching noise.

To suppress voltage ripple and high-frequency noise, a diode-bridged RC filter is placed between the power sources and the trap electrodes. This provides spike protection, noise filtering, and isolation of switching transients, crucial for protecting the stored antiprotons and maintaining the performance of resonator-based detection systems. The characteristic time constant of the RC filter is $\tau \sim 2.05\,\mu$s, giving us a cutoff frequency around 80 Hz. Therefore, we are able to filter out the RF noise of the power supply, and retain a DC-like signal for a stable electrode potential.

In order to verify the circuit met the specified requirements, the proposed circuit was simulated using LTspice. For the most realistic results, the different components were modeled (where applicable) as their real-world counterparts, shown in table 1, that were chosen for the development of the board. Moreover, the Stahl Electronics HS2000 switch and the RT HV electrodes were also modeled as shown in Fig. 6, as in reality, these components have some non-negligible resistance and capacitance that plays a crucial role when aiming for nanosecond regime functionality.

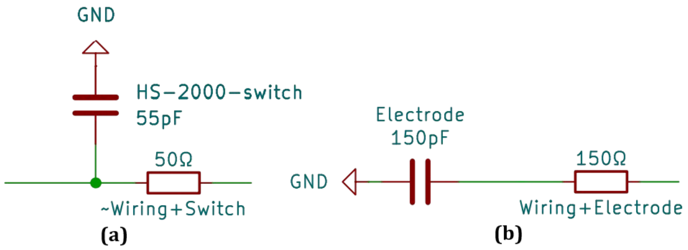

Fig. 6 Models of **(a)** the Stahl Electronics HS-2000 HV switch and **(b)** the RT HV electrodes, used to simulate the circuit in LTspice. The chosen values were known from quick measurements in the lab.

Initially, the rise time of the output voltage was found to be in the microsecond regime, as shown in Fig. 7a, primarily due to the intrinsic capacitance of the HV switch, which delayed charge delivery to the US-HV electrode. To compensate for this, a buffer capacitor (**C1**) was added right before the switch. Simulations showed that increasing the capacitance of **C1** the rise time, as shown in Fig. 7b, with saturation observed around 100 nF, giving a voltage rise time of ∼50.56 ns at the output. This value was thus selected as optimal.

The effect of adding buffer capacitors in-between a power supply and a switch was not as significant, but still noticeable for the BSHV-400 power supplies. Therefore, after running similar simulations for each, capacitors **C2**, **C4** and **C5** were added for redundancy, with their optimal value found to be around 10 nF.

The components used for the development of this circuit are summarized in Table 1. Component selection prioritized high-voltage tolerance $\gtrsim$2 kV , fast response times, and safety. Surface-mount resistors and capacitors with sufficient spacing and power rratings were used to ensure robustness under high electric fields. Schottky diodes were chosen for their low forward voltage and fast response, ensuring minimal delay or ringing during switching events.

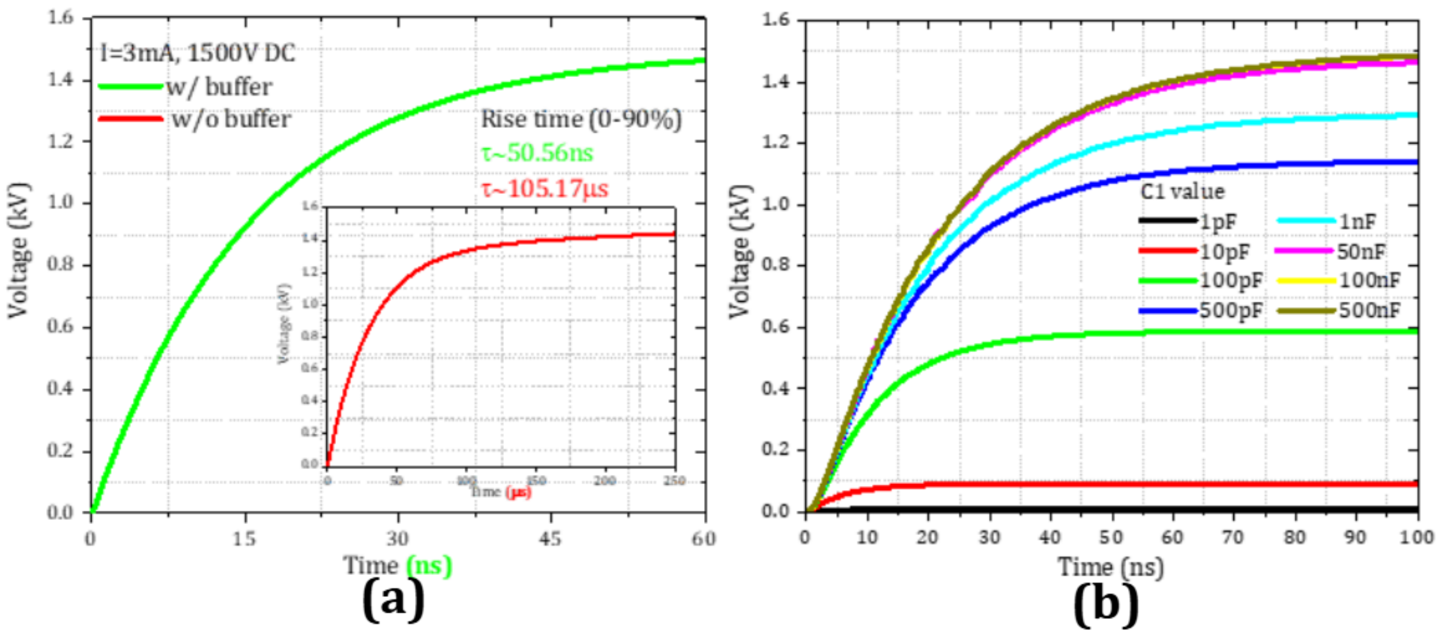

Fig. 7 Simulation of the voltage at the US-HV electrode **(a)** with and without C1 (at the optimal value) and **(b)** at different values of C1, with 1.5 kV at the input. The simulations were ran on the circuit shown in Fig. 5 in LTspice, and each component was modelled to have the characteristics of the actual component that would be used, shown in table 1, where the software allowed. The switch and electrode were modeled as shown in Fig. 6.

Schematic reference	**Component**	**Key specs**
R1-R8	KOA Speer Electronics, Inc. HV732BTTD8203F	≥1.5 kV rated, 1206 body, exact value 820 kΩ, 330 mW power rating
C1	CAP CER 2220 2000VDC 100NF 10% X7R (2R1)	100 nF, 2 kV X7R, 2220 body (largest available), low series resistance (<100 mΩ)
C2-C6	CAP CER 2220 10NF 2000V X7R 10%	10 nF, 2 kV X7R, 2220 body (largest available), low series resistance (<30 mΩ)
D1-D8	DIODE ARR SCHOT 70V 70MA SOT23-3	Dual Schottky array, $V_r = 70$ V, rise time ≈ 5 ns
K1-K2	OMRON G2R-1 DC24	24 V coil, 5 kV isolation
SHV	CONN SHV JACK STR SOLDER	5 kV rated, Non-constant impedance
BNC	CONN BNC RCPT STR 50 OHM SOLDER	500 V rated, 50 Ω impedance
Box	Rose Enclosures 042020070	Metal-Aluminum box, 200.0 × 200.0 × 72.5 mm (L × W × H)

Tab. 1 Summary of the main electrical and mechanical components selected for the circuit developed to switch between fast and low-noise high-voltage supplies during antiproton trapping. All components were sourced via Digi-Key and were chosen for their high voltage ratings, fast switching performance, and suitability for integration into the BASE reservoir trap system.

The full schematic was then translated into the PCB layout shown in Fig. 8, with particular attention paid to trace width, pad spacing, and curved routing to avoid sharp corners. The final layout reflects the physical and electrical constraints discussed previously and is compatible with BASE's existing RT infrastructure.

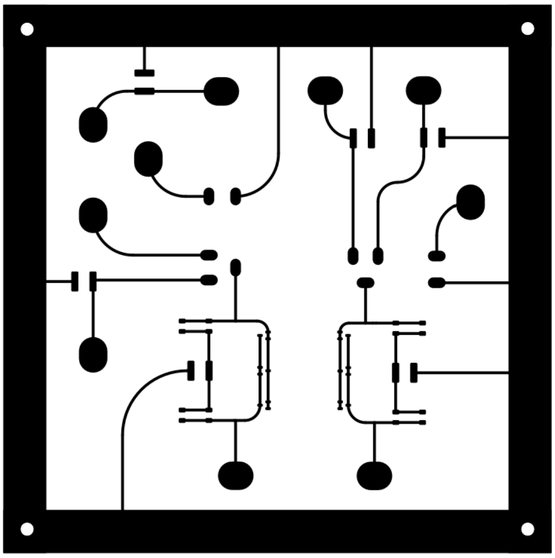

Fig. 8 Front view of the exposed copper (black) layer of the PCB. The copper traces connecting pads to components are covered by a solder mask and the exposed copper border is grounded.

The boards are 155×155×1.55 mm (L × W × H), with approximately 10 mm of clearance between HV components. The copper traces connecting the different components are 0.8 mm wide and are covered by a solder mask for increased isolation and to safeguard against potential short-circuits from solder. Oval shaped pads were implemented for connecting the board to the different power sources through wires connecting the pad and the corresponding SHV or BNC connection.

Figure 9**(f)** shows the actual prototype PCB developed as part of this project. The PCB itself is mounted inside a Metal-Aluminum enclosure, referenced in table 1, which is connected to ground, allowing grounding of the board components by connecting them to the exposed copper borders.

Figures 9**(a-d)** show side-views of the switch box and the different connections to the board. Specifically, 9**(a)** shows the main inputs, with the "HVS IN" and "HVP IN" connections referring to the connections to the CAEN NDT1470 high-voltage power supply and the "HV400-CH1" connection referring to the connection to channel 1 of the lower voltage, more stable

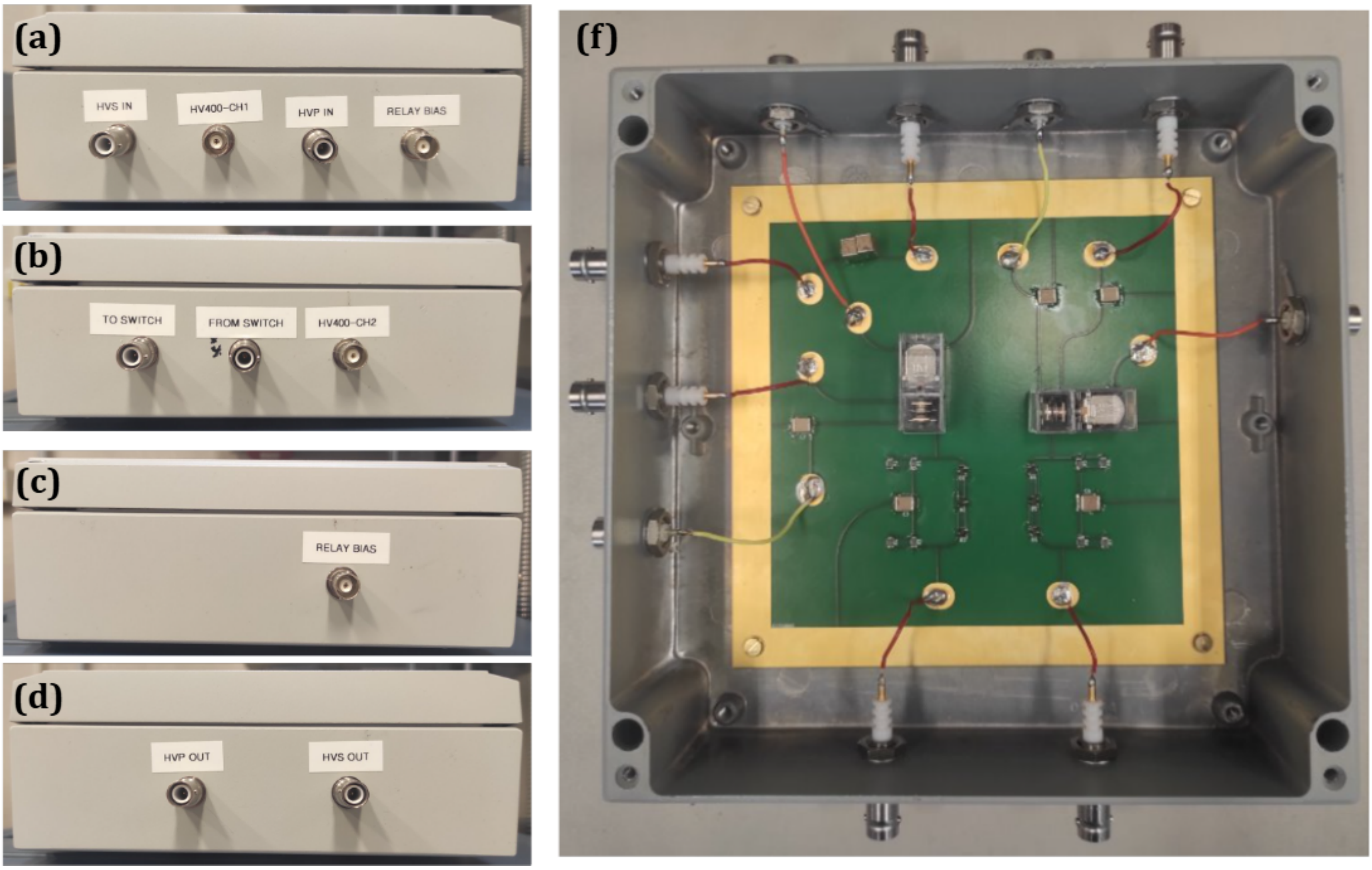

Fig. 9 Photos of the prototype switch developed during this project, with **(a-d)** side-views of the switch box, showing the different connections, as well as **(f)** a top-view of the open switch box, showcasing the assembled electronics.

BSHV-400 power supply. The connections to the fast, HV Stahl electronics switch are shown in 9**(b)**, with "TO SWITCH" referring to the negative connection of the switch, as the switch box is operated at negative voltages and switched from ground (positive connection), and "FROM SWITCH" refers to the connection to the COM channel of the switch. The "HV400-CH2" connection refers to the connection to channel 2 of the BSHV-400 power supply. The "RELAY BIAS" connections in figures 9**(a,c)** are used to switch between the higher voltage and lower voltage power supplies when appropriate, with an operating voltage of 16.8 V and a releasing voltage of 3.6 V. Lastly, figure 9**(d)** shows the output connections to the US ("HVP OUT") and DS ("HVS OUT") HV-electrodes.

Due to time constraints in the project timeline, extensive testing of the switch box under fully experimental conditions was not possible. However, preliminary tests were conducted to confirm the basic functionality of the switching circuit. Specifically, the switching function of the Stahl electronics fast HV switch was verified while connected to the switch box, as well as the response of the relays at the output when toggling between the power supplies. Oscilloscope traces confirmed that the HV switches engaged properly and redirected the output voltage as expected. While a more thorough analysis of rise/fall times, ringing, and noise performance is needed for a full qualification, these early results confirm that the switch box is functioning and able to perform the core operation required for antiproton trapping. A more extensive test of the developed switches is planned in the near future, before implementation in an actual antiproton catching phase later this year.

Fig. 10 Top-view of the three switches developed during this project, one for use at BASE, one for use at STEP and a spare one as a backup.

4 Conclusions

In this project, a high-voltage switch box was designed, simulated, and constructed to meet the demanding requirements of antiproton trapping in the BASE reservoir trap system. The developed circuit enables the delivery of fast, nanosecond-scale high-voltage pulses for the catching phase, followed by low-noise operation for long-term storage. Careful attention was given to minimizing switching delays, suppressing noise, and ensuring electrical robustness under high-voltage operation.

Although only preliminary tests were conducted due to limited time, the results confirm that the switching functionality operates as intended. These tests showed reliable toggling between fast and low-noise high-voltage supplies, validating the core design principles. More extensive characterisation, including rise/fall time measurement under operational voltages, noise spectrum analysis, and long-term stability testing, are the immediate next tests before qualification before full deployment in catching phases in the near future.

Following the promising test results, three identical switch boxes were built, one designated for use in the BASE experiment at CERN, one for the BASE-STEP collaboration, and a third kept as a spare. These units are now ready for characterisation tests and integration into the respective experimental setups, where they are expected to play an important role in ensuring efficient antiproton capture and stable storage for precision measurements.

References

[1] Moritz Borchert. *The Magnetic Moment of the Antiproton*. PhD thesis, Ruprecht-Karls-Universität Heidelberg, 2020. CERN-THESIS-2020-228.

[2] H. Nagahama, C. Smorra, S. Sellner, J. Harrington, T. Higuchi, M. J. Borchert, T. Tanaka, M. Besirli, A. Mooser, G. Schneider, K. Blaum, Y. Matsuda, C. Ospelkaus, W. Quint, J. Walz, Y. Yamazaki, and S. Ulmer. Sixfold improved single particle measurement of the magnetic moment of the antiproton. *Nature Communications*, 8(1):14084, 2017.

[3] Georg Schneider. Development of a penning trap system for the high precision measurement of the antiproton's magnetic moment. Master's thesis, Johannes Gutenberg-Universität Mainz, March 2014. Referees: Prof. Dr. Jochen Walz, Dr. Stefan Ulmer.

[4] CAEN S.p.A. Caen ndt1470 - 4 ch reversible 8 kv/3 ma hv power supply. https://www.caen.it/products/ndt1470/, 2025. Accessed: 2025-07-23.

[5] Stahl Electronics. Price list february 2021 – april 2021 (€-version, valid for end users in europe and north america). https://www.stahl-electronics.com/bilder/Price_List_Feb_to_April_2021.pdf, 2021. Accessed: 2025-08-07.

[6] Stefan Ulmer, Arno Mooser, Hidetoshi Nagahama, Stefan Sellner, and Christian Smorra. Challenging the standard model by high-precision comparisons of the fundamental properties of protons and antiprotons. *Philosophical Transactions of the Royal Society A*, 376(2139), 2018.

[7] Stefan Ulmer, Christian Smorra, Barbara M. Latacz, Fatma Abbass, Ino Ahrens, Bela P. Arndt, Amado Bautista-Salvador, Julia-Aileen Coenders, Juan Manuel Cornejo, Satoshi Endoh, Stefan R. Erlewein, Philip Geissler, Tomoka Imamura, Julia I. Jäger, Hanna Klett, Marcel Leonhardt, Teresa Meiners, Peter Micke, Anton Siebert, Daniel Schweitzer, Simon Stahl, Paula Schöps, Tesse Tiemens, Ann Thomas, Frederik Völksen, Elise Wursten, Christian Will, Hüseyin Yildiz, Klaus Blaum, Jack A. Devlin, Yasuyuki Matsuda, Christian Ospelkaus, Wolfgang Quint, Anna Soter, Jochen Walz, and Yasunori Yamazaki. BASE - Annual Report 2024. Annual Report SPSC-SR-361, CERN, September 2025.